Article

Enhancement of Corneal Visibility in Optical Coherence Tomography Images Using Corneal Adaptive Compensation

Michaël J. A. Girard[1,2], Marcus Ang[2], Cheuk Wang Chung[1], Mohamed Farook[2], Nick Strouthidis[2,3], Jod S. Mehta[2,4], and Jean Martial Mari[5]

[1] In vivo Biomechanics Laboratory, Department of Biomedical Engineering, Faculty of Engineering, National University of Singapore, Singapore
[2] Singapore Eye Research Institute, Singapore National Eye Centre, Singapore
[3] NIHR Biomedical Research Centre, Moorfields Eye Hospital NHS Foundation Trust & UCL Institute of Ophthalmology, London, UK
[4] Department of Clinical Sciences, Duke-NUS Graduate Medical School, Singapore
[5] Université de la Polynésie française, Tahiti, French Polynesia

Purpose: To improve the contrast of optical coherence tomography (OCT) images of the cornea (post processing).

Methods: We have recently developed standard compensation (SC) algorithms to remove light attenuation artifacts. A more recent approach, namely adaptive compensation (AC), further limited noise overamplification within deep tissue regions. AC was shown to work efficiently when all A-scan signals were fully attenuated at high depth. But in many imaging applications (e.g., OCT imaging of the cornea), such an assumption is not satisfied, which can result in strong noise overamplification. A corneal adaptive compensation (CAC) algorithm was therefore developed to overcome such limitation. CAC benefited from local A-scan processing (rather than global as in AC) and its performance was compared with that of SC and AC using Fourier-domain OCT images of four human corneas.

Results: CAC provided considerably superior image contrast improvement than SC or AC did, with excellent visibility of the corneal stroma, low noise overamplification, homogeneous signal amplification, and high contrast. Specifically, CAC provided mean interlayer contrasts (a measure of high stromal visibility and low noise) greater than 0.97, while SC and AC provided lower values ranging from 0.38 to 1.00.

Conclusion: CAC provided considerable improvement compared with SC and AC by eliminating noise overamplification, while maintaining all benefits of compensation, thus making the corneal endothelium and corneal thickness easily identifiable.

Translational Relevance: CAC may find wide applicability in clinical practice and could contribute to improved morphometric and biomechanical understanding of the cornea.

Introduction

While optical coherence tomography (OCT) imaging has been used increasingly to monitor retinal disorders, there has been a growing interest for its use in corneal applications in recent years. Clinically, anterior segment OCT (ASOCT) has shown great promise in a variety of indications, for example, in (1) mapping corneal topography and tomography with high resolution,[1] (2) evaluating corneal wounds, incisions, scars, inflammation or infective lesions, (3) assessing the posterior cornea in terms of topography and structural changes (e.g., diagnosing Descemet's membrane detachment), and in (4) evaluating and monitoring structural changes following corneal transplants and corneal refractive surgeries.[2] As ASOCT hardware and software continues to improve, we are witnessing an increasing use of the ASOCT in
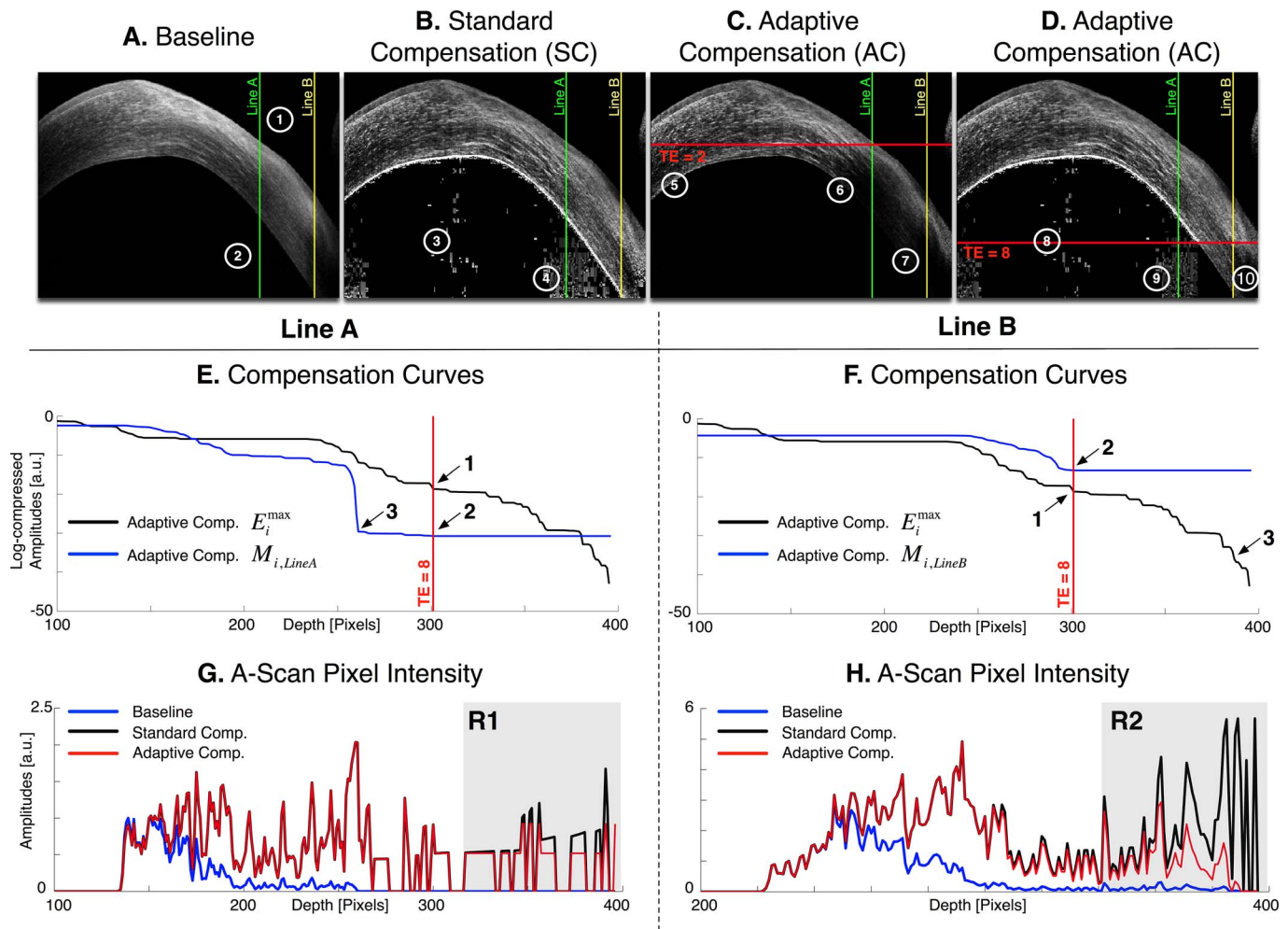
Figure 1. **Images (A–D):** Baseline, standard, and adaptive compensation images with a contrast exponent of $n = 2$ (cornea of subject #4). Maximum penetration depths i^{stop} (*horizontal redlines*) are shown for two different threshold exponents (TE = 2 and TE = 8); region 1: shallow region usually well handled by standard and adaptive compensations; region 2: deeper region overamplified by the standard method (regions 3, 4), and either underamplified by the adaptive approach (regions 5–7), or overamplified (regions 8, 9) and underamplified (region 10). In the case of tissues being both shallow and deep-seated in the image, a maximum penetration depth estimation cannot prevent overamplification while preserving deep tissues. *Vertical lines* indicate the A-Scans A ($j = 571$; in *green*) and B ($j = 713$; in *yellow*) used for (E–H). **Plots (E, F):** Examples of global penetration profile ACE_i^{max} and compensation curve $ACM_{i,j}$ for the A-scans A (E) and B (F); *Arrow 1*: maximum penetration depth i^{stop} estimation; *Arrow 2*: adaptive amplification stopped at i^{stop}; *Arrow 3*: depths where amplification should be stopped (as those correspond to the corneal endothelium). For adaptive compensation, i^{stop} is fixed despite the presence of shallow region (E) and deeper region (F) tissues. **Plots (G, H):** examples of baseline $I_{k,j}$ and compensated A-scans $I_{i,j}^{SC}$, $I_{i,j}^{AC}$ and $I_{i,j}^{CAC}$ for the lines A (E) and B (F). R1: region overamplified by both standard and adaptive methods; R2: region underamplified by the adaptive compensation approach.

daily clinical practice, as well as for 'real-time' intraoperative assessments.[3]

However, corneal images acquired with OCT suffer from the very same visibility artifacts observed in retinal or optic nerve head images, which are the direct result of light attenuation and sensitivity falloff with depth.[4,5] We have previously proposed standard compensation (SC) techniques (post processing) to remove the deleterious effects of light attenuation and thus considerably improve tissue visibility and con-

trast in OCT images (see reference 4 for the definition of contrast values). Our latest adaptive compensation (AC) technique was also able to limit noise over-amplification arising from processing.[6] While these techniques found applications in the choroid,[7] optic nerve head,[4,6,8–10] and even coronary artery OCT images[11,12] with a single, easily set and checked, parameter to encompass many different imaging situations, an initial assessment showed poor applicability to ASOCT images of the cornea (Fig. 1). This

is because the cornea is prolate in shape, biomechanically heterogeneous, and of varying thickness. Thus, ASOCT A-scans of an individual cornea exhibits signal attenuation at varying depths, thus emphasizing the need for 'local' image processing (as opposed to 'global' image processing).

In this study, we propose a novel post-processing algorithm, namely corneal adaptive compensation (CAC), which can considerably improve the image quality of corneal ASOCT images. Its performance is established herein and compared with SC and AC.

Methods

Standard Compensation

Standard compensation is a post-processing technique that can be applied to OCT images under the assumptions that light attenuation and backscattered light are proportional, and that A-scan signals are fully attenuated at infinite depth.[4] Using SC, a compensated image can be produced through pixel intensity amplification, theoretically without depth limitation. Such amplification aims to enhance 'weak signals' and is progressively increased with depth using Equation 1a to produce the compensated intensities $I_{i,j}^{SC}$. Here, $M_{i,j}$ is the compensation profile ($1/M_{i,j}$ being the amplification factor) for each A-scan j and A-scan pixel at depth i ($i = 0$: top of the image; $i = N$: bottom of the image); n is an exponent that controls contrast (typically 1 or 2).[4]

$$
\begin{cases}
I_{i,j}^{SC} = \dfrac{I_{i,j}^n}{2.M_{i,j}} & (1a) \\[2em]
M_{i,j} = \displaystyle\sum_{k=i}^{N} I_{k,j}^n & (1b)
\end{cases}
$$

While SC has been demonstrated to considerably improve OCT image quality, it is hampered by the presence of undesirable noise overamplification in the deepest image regions. This is because $I_{i,j}^n$ tends toward noise and $M_{i,j}$ tends toward zero at high depth, thus limiting the overall performance of SC.

Adaptive Compensation/Standard Compensation

Adaptive compensation was developed to remove noise over-amplification at high depth[6] and is briefly recalled in Equation 2. AC first compares all A-scans and estimates the maximum penetration depth i^{stop} (Equation 2c) using the global maximum energy profile of all A-scans (Equation 2b). Then AC computes the standard compensation profile $I_{i,j}^{AC}$ for each A-scan down to the estimated depth i^{stop} (Equations 2d, e), and then maintains the compensation coefficient $M_{i,j}$ for each A-scan.

$$
\begin{cases}
E_{i,j} = \displaystyle\sum_{k=i}^{N} \left[I_{k,j}^n \right]^2 & (2a) \\[1.5em]
E_i^{max} = max_j\, E_{i,j} & (2b) \\[1em]
i^{stop} = i / E_i^{max} < 10^{-TE}.E_0^{max} & (2c) \\[1em]
M_{i,j} =
\begin{cases}
\displaystyle\sum_{k=i}^{N} I_{k,j}^n & i < i_{stop} \\[1.5em]
\displaystyle\sum_{k=i_{stop}}^{N} I_{k,j}^n & i \geq i_{stop}
\end{cases} & (2d) \\[3em]
I_{i,j}^{AC} = I_{i,j}^n / 2.M_{i,j} & (2e)
\end{cases}
$$

We have previously shown that the energy threshold exponent or TE (that controls i^{stop}) can be easily chosen, as only a very small part of the energy remains at the bottom of shallow tissue images. For such images, noise overamplification can be efficiently removed (e.g., providing better visibility of the posterior lamina cribrosa surface in OCT images of the human optic nerve head).[6,8] Examples of global energy and compensation profiles are shown in Figures 1E and 1F for the two A-scans (lines A and B) in Figures 1A through 1D. The compensation coefficients $M_{i,j}$ are maintained constant for i greater than i^{stop} using TE = 8 (Figs. 1E, F, arrow 2). Note that i^{stop} is the maximum penetration depth and corresponds to the point where only $10^{-TE} = 10^{-8}$ of the initial value E_0^{max} of the global energy profile E_i^{max} remains (Figs. 1E, F, arrow 1). Maintaining the compensation coefficients constant past a given limit results in a regularization of the deeper part of the signals, which can be observed in Figures 1G and 1H, where the two A-scan signals (baseline, SC, and AC) are plotted as a function of depth. In Figure 1G (region R1) the baseline signal is essentially background noise. For i greater than $i^{stop} = 301$, the AC signal is not amplified anymore thus resulting in less noise overamplification than with SC. Although stopping AC signal amplification at arrow 3 in Figure 1E would be desirable as this corresponds to the corneal endothelium, stopping further at arrow 2 still ensures some level of noise overamplification control for AC as opposed to SC.

Corneal Adaptive Compensation

In many imaging situations (e.g., ASOCT corneal imaging), biological tissues can be present in both shallow and deep regions of the image. For such images, SC would still overamplify signal at high depth, but AC would stop amplifying beyond a global limit i^{stop} as illustrated in Figures 1F and 1H. In Figure 1F (TE = 8), the A-scan would ideally require further amplification down to the end of the line (Fig. 1F, arrow 3 corresponding to the corneal endothelium), but AC maintains $M_{i,j}$ constant prematurely (at arrow 2). Choosing a larger TE value (a smaller threshold) would not solve the problem, as the A-scans containing only noise in the deep regions would be amplified as well. The early maintenance of the $M_{i,j}$ values translates in Figure 1H to the underamplification of the AC signal (region R2).

Therefore, the presence of variation in tissue depth in the image requires the estimation of a compensation limit, which is dynamically adapted to the local energy profile, by estimating a maximum penetration depth i_j^{stop} for each A-scan j. To that end, each energy line $E_{i,j}$ (Equation 3a) must be individually thresholded (Equation 3b). Note that the use of very small threshold values (as with AC) ensures deep tissue signal compensation while preventing noise overamplification.

$$
\begin{cases}
E_{i,j} = \sum_{k=i}^{N} \left[I_{k,j}^n \right]^2 & (3a) \\
i_j^{stop} = i / E_{i,j} < 10^{-TE}.E_{0,j} & (3b) \\
M_{i,j} = \begin{cases} \sum_{k=i}^{N} I_{k,j}^n & i < i_j^{stop} \\ \sum_{k=i_j^{stop}}^{N} I_{k,j}^n & i \geq i_j^{stop} \end{cases} & (3c) \\
I_{i,j}^{CAC} = I_{i,j}^n / 2.M_{i,j} & (3d)
\end{cases}
$$

The novel corneal adaptive compensation (CAC) technique, developed in the first place for ASOCT corneal images, is fully described by Equation 3. Once individual A-scan maximum penetration depths i_j^{stop} have been computed, the same regularization of the compensation profile $M_{i,j}$, as in AC, is performed (Equation 3c) to generate a CAC image $I_{i,j}^{CAC}$. Note that to obtain compensated intensities, the compensation equations are discretized with a spatial

sampling Δ equal to 1.[4] When the compensated intensities are divided by the physical value of Δ, they represent a quantitative measure of light attenuation.[13]

Application and Performance of CAC

Fourier-domain ASOCT images of the cornea (horizontal B-scan; ×20 signal averaging) were acquired from the right eye of four human subjects (2 healthy eyes and 2 eyes exhibiting corneal scars) with a commercially available device (RTVue; Optovue, Inc., Fremont, CA). Imaging was performed at the Singapore National Eye Centre, Singapore, and this retrospective study was conducted with the approval from the SingHealth institutional review board, Singapore. All subjects gave informed oral consent and were treated in accordance with the Declaration of Helsinki. All patient records were anonymized and deidentified prior to analysis.

Before applying compensation (SC, AC, or CAC), each ASOCT image was transformed (i.e., uncompressed) to its initial raw format I^{Raw} using the following equation:

$$
I_{i,j}^{Raw} = \left(\frac{I_{i,j}^{Compr}}{255} \right)^4 \qquad (4)
$$

where I^{Compr} is the original compressed image obtained from the RTvue system. For visualization and comparison purposes, all images were then transformed back to their compressed format using the following equation:

$$
I_{i,j}^{Compr} = 255 \sqrt[4]{I_{i,j}^{Raw}} \qquad (5)
$$

Using the aforementioned corneal ASOCT images, we first qualitatively assessed the performance of CAC and compared it with that of AC for various TEs when pertinent and with contrast exponents (CEs) of 1 (slight contrast enhancement) or 2 (high contrast enhancement). The performance of CAC was also assessed quantitatively by computing the inter-layer contrast[4] defined as:

$$
\text{inter-layer contrast} = \left| \frac{I_3 - I_4}{I_3 + I_4} \right| \qquad (6)
$$

where I_3 is the mean pixel intensity of a region of interest (ROI) located within the corneal stroma, and I_4 is that within a deeper region of the anterior chamber (i.e., background). Here, the inter-layer contrast is a measure of corneal endothelium visibility

Adaptive Compensation (Previous Algorithm)

Corneal Adaptive Compensation (New Algorithm)
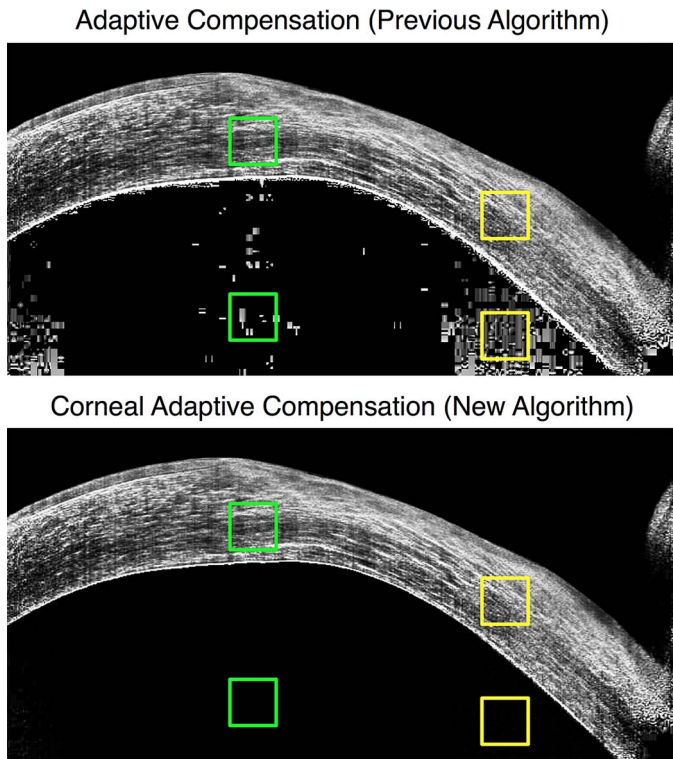
Figure 2. ROIs used for interlayer contrast calculations at two different vertical locations (central ROI pair in *green*, peripheral ROI pair in *yellow*) for a given corneal ASOCT image processed with AC (*top*) or CAC (*bottom*).

Baseline (Subject #1)

Figure 3. Baseline, AC (low and high TE), and CAC images of a healthy cornea (subject 1) for 2 CE values (*left column*: CE = 1; *right column*: CE = 2). Improper stromal illumination is observed in the baseline images (*first row*; image duplicated for better illustration). AC (with low TE; *third row*) resulted in noise over-amplification (*central region*) and signal underamplification at the periphery. AC (with high TE; *fourth row*) resulted in improved illumination, but at the cost of high noise overamplification near the corneal endothelium (*see inlets*) and in the anterior chamber. CAC (*second row*) provided the best results with proper illumination, no signal underamplification, and minor noise overamplification. ROIs pairs used for interlayer contrast calculations are shown in *green* (*central location*) and in *yellow* (*peripheral location*). CE, contrast enhancement.
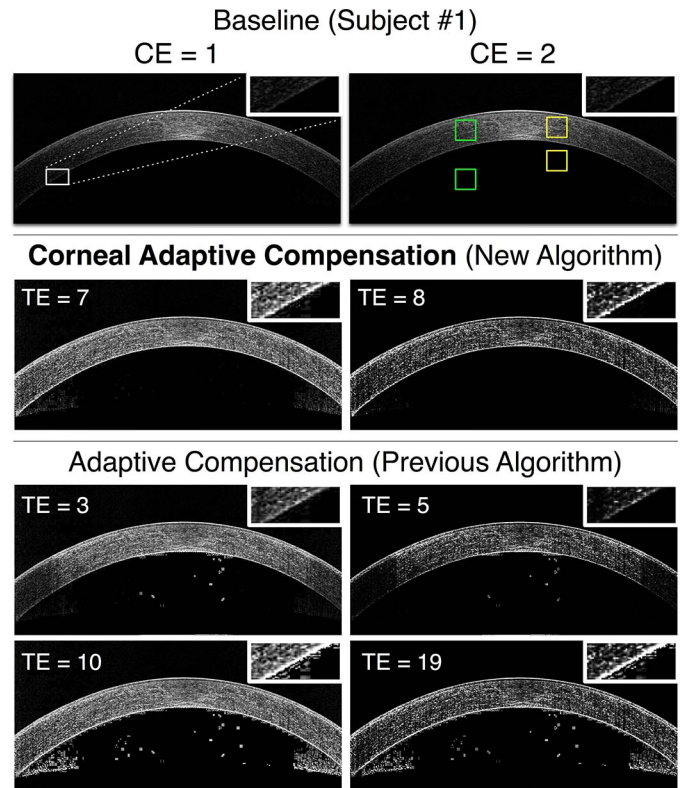
that varies between 0 (poor visibility) and 1 (high visibility). It was calculated at two different locations (central and peripheral) that are typically over-amplified by SC and AC (Fig. 2). The ROIs were 60 × 60 pixels in size for all subjects. Finally, for a given subject, the exact same ROI locations were used to calculate the interlayer contrast for the SC, AC, and CAC images as illustrated in Figure 2.

Results

Qualitative Assessment of CAC and Comparison With AC

All baseline corneal ASOCT images exhibited nonuniform illuminations with especially poor tissue visibility at the cornea periphery (Figs. 3–6). Additionally, baseline images from unhealthy subjects exhibited shadowing of the corneal stroma due to scarring (Figs. 5, 6).

For all images, AC with low TE values restored corneal stroma homogeneity in the central region but not at the cornea periphery where the signal remained poor. Furthermore, noise overamplification was present in all images, which considerably affected corneal endothelium visibility. AC with high TE values provided excellent homogeneity of the corneal stroma in all subjects, but at the cost of strong and unwanted noise overamplification in the deepest corneal layers. These results were true for both CE values that were tested (1, 2).

CAC provided considerably superior image contrast than AC did with excellent corneal stroma visibility and low noise overamplification, thus making corneal endothelium and corneal thickness easily identifiable. Further, CAC with CE = 2 allowed contrast enhancement without providing additional noise.
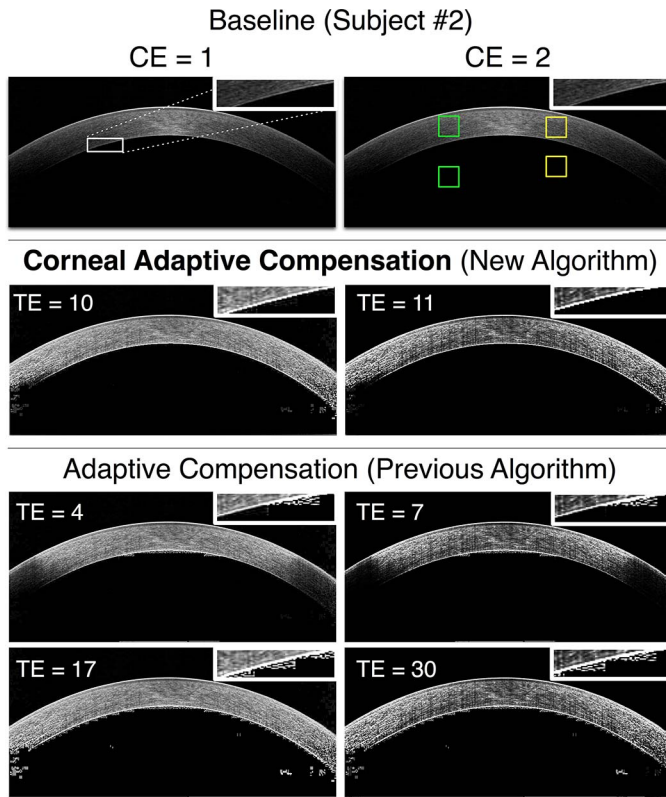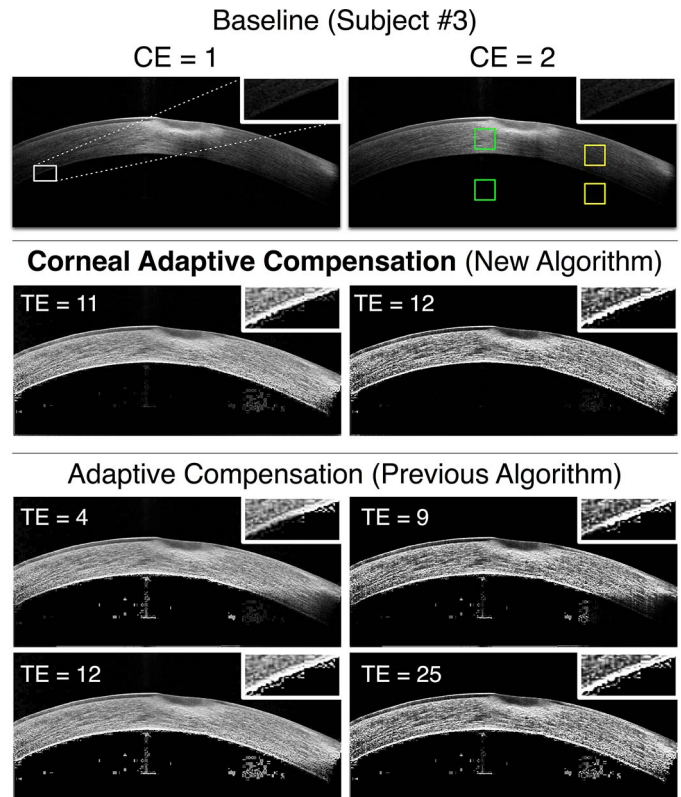
Figure 4. Baseline, AC (low and high TE), and CAC images of a healthy cornea (subject 2) for 2 CE values (*left column*: CE = 1; *right column*: CE = 2). The caption from Figure 3 also applies to this Figure.

Figure 5. Baseline, AC (low and high TE), and CAC images of an unhealthy cornea exhibiting scarring at the apex (subject 3) for 2 CE values (*left column*: CE = 1; *right column*: CE = 2). The caption from Figure 3 also applies to this Figure.

Quantitative Assessment of CAC and Comparison With SC and AC

A CAC image of the cornea is shown in Figure 7D, along with the maximum penetration depths i_j^{stop} for each A-scan (represented as a red dashed line that matches the corneal endothelium boundary). CAC does not produce signal overamplification (Fig. 7D, regions 6, 7) as observed with SC (Fig. 7B, regions 1, 2) and with AC (Fig. 7C, regions 3, 4), nor signal underamplification (Fig. 7D, region 8) as observed with AC (Fig. 7C, region 5).

Compensation profiles are compared between the different techniques (SC, AC, and CAC) for 2 A-scans in Figures 7E and 7F. For both shallow and deep tissue A-scans, the CAC limit i_j^{stop} (arrow 5) is consistently close to the 'ideal' compensation limit (arrow 3) represented by the corneal endothelium, while the AC limit i^{stop} (TE = 8) remains the same (arrow 2).

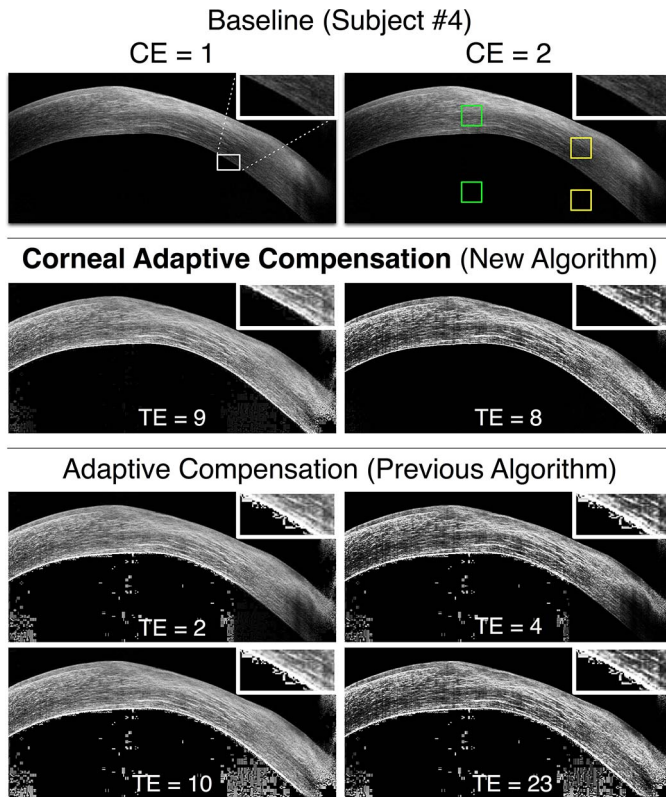Improved CAC performance is further illustrated in Figures 7G and 7H where baseline, SC, AC, and CAC intensity signals are plotted for 2 A-scans. In region R1, CAC efficiently stopped the amplification below the corneal endothelium, while in region R2, the compensation was carried out until the remaining energy was so small that the amplification was stopped, thus preventing saturation.

The inter-layer contrasts C1 and C2 obtained respectively from the region pairs illustrated in Figure 2 are provided in Table 1 (for SC, AC with $2 \leq TE \leq 30$, and CAC with $7 \leq TE \leq 12$) for all four subjects. SC and AC yielded inter-layer contrasts ranging from 0.38 to 1.00, with mean coefficients of variation of 18.15% for AC, and 32.14% for SC. CAC performed considerably better, with inter-layer contrasts all exceeding 0.97 for a wide range of TE values (between 7 and 12), and with a low mean coefficient of variation (0.48%).

Discussion

In this study, we have proposed a novel compensation algorithm that can considerably enhance the contrast of corneal images captured with ASOCT.

Baseline (Subject #4)
CE = 1   CE = 2

Corneal Adaptive Compensation (New Algorithm)
TE = 9   TE = 8

Adaptive Compensation (Previous Algorithm)
TE = 2   TE = 4
TE = 10   TE = 23

Figure 6. Baseline, AC (low and high TE), and CAC images of an unhealthy cornea exhibiting scarring at the apex (subject 4) for 2 CE values (*left column*: CE = 1; *right column*: CE = 2). The caption from Figure 3 also applies to this Figure.
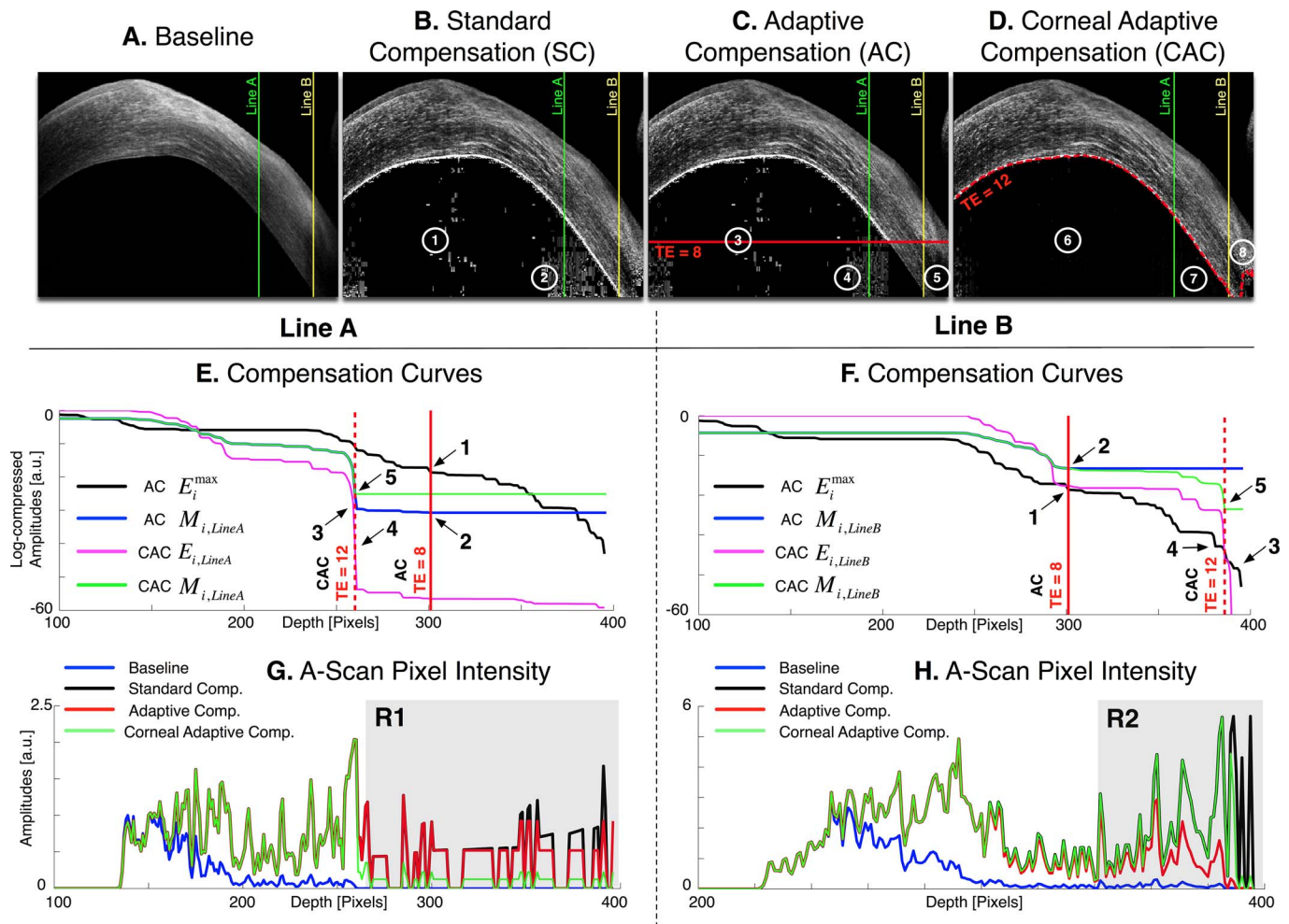
The CAC algorithm was shown to correct for light attenuation artifacts without introducing noise over-amplification, and was found to be superior to our previous implementations known as SC or AC.

Corneal ASOCT images suffer from the same light attenuation artifacts as retinal or optic nerve head images including degradation of image quality (e.g., from corneal scaring) and nonuniform stromal illumination. To the best of our knowledge, no post-processing solutions have yet been proposed to correct these artifacts. SC and AC were first considered as strong candidates to enhance the contrast of ASOCT images of the cornea as their performance has been thoroughly tested in OCT images of the optic nerve head.[4,6] However, when these compensation algorithms were applied to corneal images (Fig. 1), either noise overamplification was observed in an entire given image (SC or AC with high TE values), or in parts but together with regions of signal underamplification (AC with small TE values). Overall, this suggested the inapplicability of either SC or AC for ASOCT images of the cornea.

Our new algorithm, CAC, was able to provide major improvements compared with baseline, SC, or AC images. Firstly, CAC was able to provide homogeneous stromal illumination compared with baseline images. This represents a considerable advantage since the peripheral corneal stroma in baseline images is often poorly visible (see inlets of Figs. 3–6), thus limiting the ability to detect corneal defects from a single B-scan acquisition. Secondly, CAC was not affected by noise overamplification in the vicinity of the corneal endothelium or within the anterior chamber (as observed with SC and AC with high TE). Those results are confirmed quantitatively by comparing the stroma with noise interlayer contrasts C1 and C2 in two different locations (central and border zones) of the four corneal images. Specifically, SC and AC provided interlayer contrasts ranging from 0.38 to 1.00, with mean coefficients of variation of 18.15% (AC) and 32.14% (SC). In comparison, CAC achieved interlayer contrasts all above 0.97, with a mean coefficient of variation of 0.48% suggesting low noise and high corneal stroma/ endothelium visibility. Thirdly, CAC was not affected by signal underamplification (as observed with AC with low TE) suggesting that compensation is properly applied to all corneal regions. Finally, CAC with CE = 2 was able to provide improved contrast without generating additional noise. Such an option could offer clinicians improved detection of heterogeneous corneal features such as may be encountered in cases with corneal scars.

It is also interesting to note that, with CAC, the adaptive limit i_j^{stop} (the boundary when compensation is stopped in Equation 3b) coincides with the corneal endothelium boundary. This is an ideal situation as no further signal amplification should be required past the corneal endothelium. Therefore, CAC could also be used to automatically segment the corneal endothelium, an important advantage for morphometric or biomechanical characterization of the cornea in vivo.[14] It should be emphasized that corneal endothelium edge detection is a direct outcome of CAC, and no prior segmentation is actually required for CAC to operate.

Our study has important clinical implications. Today, corneal diseases are still one of the most common causes of vision loss and irreversible blindness.[15,16] It is estimated that more than 180 million people worldwide suffer from visual impairment from corneal disease, and over 10 million patients with blindness from ocular surface scarring.[15] Corneal transplantation still remains the main meth-

A. Baseline

B. Standard Compensation (SC)

C. Adaptive Compensation (AC)

D. Corneal Adaptive Compensation (CAC)

Line A

Line B

E. Compensation Curves

F. Compensation Curves

G. A-Scan Pixel Intensity

H. A-Scan Pixel Intensity

Figure 7. **Images (A–D):** Baseline, standard, adaptive, and corneal adaptive compensation images with a contrast exponent of $n = 2$ (cornea of subject #4). The adaptive maximum penetration depth i^{stop} is plotted as a *horizontal red line* (for TE = 8), and the corneal adaptive maximum penetration depth i_j^{stop} as a *dashed red curve* (for TE = 12); Regions 1 to 4: areas over-amplified by the standard and adaptive compensation methods; Regions 6 to 8: over- and underamplifications have been avoided using depth-dependent amplification limits. *Vertical lines* indicate the A-scans A ($j = 571$; in *green*) and B ($j = 713$; in *yellow*) used for (E–H). **Plots (E, F):** examples of global penetration profile (ACE_i^{max}), adaptive compensation curve ($ACM_{i,j}$), corneal penetration profile ($CAC\ E_{i,j}$) and corneal compensation curve ($CACM_{i,j}$) for A-scans A (E) and B (F); *Arrow 1*: maximum penetration depth i^{stop} estimated from the adaptive global-penetration profile; *Arrow 2*: adaptive compensation stopped at i^{stop}; *Arrow 3*: depths where amplification should be stopped (as those correspond to the corneal endothelium); *Arrow 4*: corneal adaptive maximum penetration depth i_j^{stop} estimated using the line-dependent penetration profile $CAC\ E_{i,j}$; *Arrow 5*: corneal amplification $CACM_{i,j}$ stopped at i_j^{stop}. This latter is automatically adjusted for shallow (E) and deeper tissues (F). **Plots (G, H):** Examples of baseline $I_{k,j}$ and compensated A-Scans $I_{i,j}^{STD}$, $I_{i,j}^{AC}$, and $I_{i,j}^{CAC}$ for the lines A (E) and B (F). R1: region overamplified by both standard and adaptive methods, but correctly handled by the corneal adaptive approach; R2: region underamplified by the adaptive compensation approach, but well amplified by the corneal adaptive compensation.

od for restoring vision, once corneal clarity is affected. Recent developments in surgical techniques have enabled surgeons to perform selective replacement of the diseased layer of the cornea, which has led to improved corneal transplant survival and surgical outcomes. Thus, the demand for high-resolution imaging to consistently identify corneal layers, and objective quantification of corneal pathology has increased exponentially. Imaging and objective iden-

tification of each diseased layer of the cornea will enable surgeons to plan targeted replacement of that corneal tissue.[17] While ASOCT is currently used to assess corneal and anterior segment parameters in healthy population subjects,[18,19] with CAC this could also lead to improved visualization of corneal structure, lesions, and corneal measurements even in patients with corneal edema, infection, or scarring. Such information would be useful to evaluate corneal

Table. Inter-Layer Contrasts (Across the Corneal Endothelium) Measured at Two Different Vertical Locations C1 (Central Region) and C2 (Peripheral Region) for Four Subjects (1 ASOCT Image Per Subject)

TE	ROI Pair	Subject 1	2	3	4	Mean	Std	COV %	Mean COV %
Standard									
-	C1	0.93	0.97	0.47	0.38	0.69	0.27	38.64	32.14
	C2	0.76	0.98	0.46	0.71	0.73	0.19	25.64	
Adaptive									
2	C1	1.00	1.00	1.00	1.00	1.00	0.00	0.00	18.15
	C2	1.00	1.00	1.00	1.00	1.00	0.00	0.00	
3	C1	1.00	1.00	1.00	0.80	0.95	0.09	9.13	
	C2	1.00	1.00	1.00	0.92	0.98	0.03	3.41	
4	C1	1.00	1.00	1.00	0.80	0.95	0.09	9.18	
	C2	0.92	1.00	1.00	0.90	0.96	0.05	4.77	
5	C1	1.00	1.00	1.00	0.80	0.95	0.09	9.20	
	C2	0.92	1.00	1.00	0.89	0.95	0.05	4.95	
7	C1	0.94	0.97	0.77	0.78	0.87	0.09	10.64	
	C2	0.76	0.99	0.88	0.86	0.87	0.08	9.14	
9	C1	0.94	0.97	0.77	0.55	0.81	0.17	20.87	
	C2	0.76	0.99	0.85	0.76	0.84	0.09	10.91	
10	C1	0.93	0.97	0.77	0.38	0.76	0.24	30.98	
	C2	0.76	0.99	0.84	0.71	0.82	0.10	12.58	
12	C1	0.93	0.97	0.77	0.38	0.76	0.24	30.99	
	C2	0.76	0.99	0.83	0.71	0.82	0.10	12.58	
17	C1	0.93	0.97	0.75	0.38	0.76	0.24	31.21	
	C2	0.76	0.98	0.73	0.71	0.80	0.11	13.51	
19	C1	0.93	0.97	0.55	0.38	0.71	0.25	35.67	
	C2	0.76	0.98	0.57	0.71	0.76	0.15	19.34	
23	C1	0.93	0.97	0.47	0.38	0.69	0.27	38.64	
	C2	0.76	0.98	0.46	0.71	0.73	0.19	25.64	
25	C1	0.93	0.97	0.47	0.38	0.69	0.27	38.64	
	C2	0.76	0.98	0.46	0.71	0.73	0.19	25.64	
30	C1	0.93	0.97	0.47	0.38	0.69	0.27	38.64	
	C2	0.76	0.98	0.46	0.71	0.73	0.19	25.64	
Corneal adaptive									
7	C1	1.00	1.00	1.00	1.00	1.00	0.00	0.00	0.48
	C2	0.99	1.00	1.00	1.00	1.00	0.01	0.56	
8	C1	1.00	1.00	1.00	1.00	1.00	0.00	0.01	
	C2	0.99	1.00	1.00	1.00	1.00	0.01	0.58	
9	C1	1.00	1.00	1.00	1.00	1.00	0.00	0.04	
	C2	0.99	1.00	1.00	1.00	1.00	0.01	0.58	
10	C1	1.00	1.00	1.00	1.00	1.00	0.00	0.06	
	C2	0.98	1.00	1.00	1.00	0.99	0.01	1.01	
11	C1	1.00	1.00	1.00	1.00	1.00	0.00	0.08	
	C2	0.97	1.00	1.00	1.00	0.99	0.01	1.17	
12	C1	1.00	1.00	0.99	1.00	1.00	0.00	0.46	
	C2	0.97	1.00	1.00	1.00	0.99	0.01	1.21	

Standard and adaptive compensation ($2 \leq TE \leq 30$) performed poorly, with mean coefficients of variations (COV = Std/Mean) of 18.15% and 32.14%, respectively. Corneal adaptive compensation ($7 \leq TE \leq 12$) provided excellent performance for all images, with contrasts close to 1 and a mean coefficient of variation of 0.48%. Std, standard deviation.

structure and/or lesions, monitor remodeling following Descemet stripping endothelial keratoplasty,[20] and to guide surgical procedures such as the choice of corneal transplantation,[21,22] or even type refractive surgery.[23,24]

The present CAC formulation is an alternative to the previously created AC for particular situations for which the previous compensation methods were not designed. The increased interest in contrast enhancement methods led to the necessity to process images acquired from different types of tissues. As detailed above, CAC is able to compensate when similar pixel intensity levels are present in both upper and lower parts of the images. However, in situations where mostly low pixel intensities are present at high depth (e.g., scleral intensities in optic nerve head images), there is a risk of underamplification, as most of the A-scan energies would be coming from the more superficial brighter tissues. For such situations, compensation at a global scale (with AC) is deemed more appropriate.[6] While this study increases the panel of algorithms available for improving OCT images, future research will attempt to unify all existing methods and provide a unique and automated post-processing compensation technique.

Our study was limited to one Fourier-domain OCT device (RTVue; Optovue, Inc.) with applications to four subjects. However, the scope of the present work was not to demonstrate the wide applicability of CAC, but to emphasize its improved performance with respect to SC and AC for corneal images. Also, note that the performance of CAC could be affected by certain factors such as low signal averaging and/or increased levels of noise in the anterior chamber. Current work is ongoing to further test the performance of CAC in larger groups of subjects, with various corneal disorders, using additional commercially available ASOCT devices, and with varying acquisition parameters. It should be noted that CAC may also find applicability in OCT images of the iris, lens, limbus, trabecular meshwork, and Schlemm's canal but this remains to be demonstrated.

As a final caveat, the CAC user still needs to manually choose a TE value that will provide the best performance. Such TE value is most likely subject-specific (different subjects have different corneal optical properties) and/or device specific (different OCT devices have different light sources). With the present implementation, we are unable to provide an automated TE value for a given cornea, but future work may consider such option. However, please note that a large TE range ($7 \leq TE \leq 12$) appears to provide satisfactory CAC results (Table 1), and this should facilitate the usability of CAC.

In conclusion, we describe a novel compensation algorithm, namely CAC, which can considerably enhance the contrast of ASOCT images of the cornea and improve corneal visibility. The proposed method enlarges the panel of techniques available for restoring OCT images from different regions of the eye, which could contribute to improved diagnosis and facilitate automated analysis of ocular biomechanics.[14]

Acknowledgments

Disclosure: **M.A. Girard**, None; **M. Ang**, None; **C.W. Chung**, None; **M. Farook**, None; **N. Strouthidis**, None; **J.S. Mehta**, None; **J.M. Mari**, None

References

1. Li Y, Shekhar R, Huang D. Corneal pachymetry mapping with high-speed optical coherence tomography. *Ophthalmology*. 2006;113:792–799, e792.
2. Ramos JL, Li Y, Huang D. Clinical and research applications of anterior segment optical coherence tomography - a review. *Clin Experiment Ophthalmol*. 2009;37:81–89.
3. De Benito-Llopis L, Mehta JS, Angunawela RI, Ang M, Tan DT. Intraoperative anterior segment optical coherence tomography: a novel assessment tool during deep anterior lamellar keratoplasty. *Am J Ophthalmol*. 2014;157:334–341, e333.
4. Girard MJ, Strouthidis NG, Ethier CR, Mari JM. Shadow removal and contrast enhancement in optical coherence tomography images of the human optic nerve head. *Invest Ophthalmol Vis Sci*. 2011;52:7738–7748.

<div style="writing-mode: vertical">translational vision science & technology</div>

5. Potsaid B, Gorczynska I, Srinivasan VJ, et al. Ultrahigh speed spectral/ Fourier domain OCT ophthalmic imaging at 70,000 to 312,500 axial scans per second. *Opt Express*. 2008;16:15149–15169.

6. Mari JM, Strouthidis NG, Park SC, Girard MJ. Enhancement of lamina cribrosa visibility in optical coherence tomography images using adaptive compensation. *Invest Ophthalmol Vis Sci*. 2013;54:2238–2247.

7. Gupta P, Sidhartha E, Girard MJ, et al. A simplified method to measure choroidal thickness using adaptive compensation in enhanced depth imaging optical coherence tomography. *PLoS One*. 2014;9:e96661.

8. Kim TW, Kagemann L, Girard MJ, et al. Imaging of the lamina cribrosa in glaucoma: perspectives of pathogenesis and clinical applications. *Curr Eye Res*. 2013;38:903–909.

9. Johnstone J, Fazio M, Rojananuangnit K, et al. Variation of the axial location of Bruch's membrane opening with age, choroidal thickness, and race. *Invest Ophthalmol Vis Sci*. 2014;55:2004–2009.

10. Lee EJ, Kim TW, Kim M, et al. Recent structural alteration of the peripheral lamina cribrosa near the location of disc hemorrhage in glaucoma. *Invest Ophthalmol Vis Sci*. 2014;55:2805–2815.

11. Foin N, Mari JM, Nijjer S, et al. Intracoronary imaging using attenuation-compensated optical coherence tomography allows better visualisation of coronary artery diseases. *Cardiovasc Revasc Med*. 2013;14:139–143.

12. Foin N, Mari JM, Davies JE, Di Mario C, Girard MJ. Imaging of coronary artery plaques using contrast-enhanced optical coherence tomography. *Eur Heart J Cardiovasc Imaging*. 2013;14:85.

13. Vermeer KA, Mo J, Weda JJ, Lemij HG, de Boer JF. Depth-resolved model-based reconstruction of attenuation coefficients in optical coherence tomography. *Biomed Opt Express*. 2013;5:322–337.

14. Girard MJ, Dupps WJ, Baskaran M, et al. Translating ocular biomechanics into clinical practice: current state and future prospects. *Curr Eye Res*. 2014;40:1–18.

15. Whitcher JP, Srinivasan M, Upadhyay MP. Corneal blindness: a global perspective. *Bull World Health Organ*. 2001;79:214–221.

16. Foster A, Resnikoff S. The impact of Vision 2020 on global blindness. *Eye (Lond)*. 2005;19:1133–1135.

17. Tan DT, Anshu A, Mehta JS. Paradigm shifts in corneal transplantation. *Ann Acad Med Singapore*. 2009;38:332–338.

18. Ang M, Chong W, Huang H, et al. Comparison of anterior segment optical tomography parameters measured using a semi-automatic software to standard clinical instruments. *PLoS One*. 2013;8:e65559.

19. Ang M, Chong W, Tay WT, et al. Anterior segment optical coherence tomography study of the cornea and anterior segment in adult ethnic South Asian Indian eyes. *Invest Ophthalmol Vis Sci*. 2012;53:120–125.

20. Kanellopoulos AJ, Asimellis G. Anterior-segment optical coherence tomography investigation of corneal deturgescence and epithelial remodeling after DSAEK. *Cornea*. 2014;33:340–348.

21. Ang M, Mehta JS. Deep anterior lamellar keratoplasty as an alternative to penetrating keratoplasty. *Ophthalmology*. 2011;118:2306–2307, author reply 2307.

22. Ang M, Mehta JS, Sng CC, Htoon HM, Tan DT. Indications, outcomes, and risk factors for failure in tectonic keratoplasty. *Ophthalmology*. 2012;119:1311–1319.

23. Ang M, Chaurasia SS, Angunawela RI, et al. Femtosecond lenticule extraction (FLEx): clinical results, interface evaluation, and intraocular pressure variation. *Invest Ophthalmol Vis Sci*. 2012;53:1414–1421.

24. Ang M, Tan D, Mehta JS. Small incision lenticule extraction (SMILE) versus laser in-situ keratomileusis (LASIK): study protocol for a randomized, non-inferiority trial. *Trials*. 2012;13:75.